Kovove Mater. 59 2021 379–390
DOI: 10.4149/km_2021_6_379

Hot deformation analysis of lean medium-manganese 0.2C3Mn1.5Si steel suitable for quenching & partitioning process

M. Krbaťa[1], I. Barényi[1]*, M. Eckert[1], D. Križan[2], S. Kaar[3], A. Breznická[1]

[1]*Faculty of Special Technology, Alexander Dubcek University of Trencin, Pri Parku 19, 911 06 Trenčín, Slovak Republic*
[2]*Research and Development Department, Business Unit Coil. Voestalpine Steel Division GmbH, Linz 4020, Austria*
[3]*Research and Development, University of Applied Sciences Upper Austria, Wels 4600, Austria*

Received 28 January 2021, received in revised form 24 September 2021, accepted 13 October 2021

Abstract

The paper mainly focuses on calculating and comparing a mathematical model of the deformation behaviour at high temperatures. Analysis of the high-temperature plastic behaviour of lean medium-manganese steel 0.2C3Mn1.5Si was carried out in the temperature range of 900–1200 °C and the deformation rate in the range of 0.01–10 s^{-1} to the maximum value of the true strain 0.8. Microstructural changes were observed using light optical microscopy (LOM) and scanning electron microscopy (SEM). The effect of hot deformation temperature on true stress, peak stress, and the true strain was evaluated using the flow curves. Based on these results, transformations in steel were discussed from the dynamic recovery and recrystallisation point of view. Furthermore, a present model, taking into account the Zener-Hollomon parameter, was applied to predict the true stress and strain over a wide range of temperatures and strain rates. Using constitutive equations, material parameters and activation energy for the investigated steel could be derived. Results demonstrate the use of the model for lean medium-Mn quenching and partitioning steel (Q&P) compositions in hot deformation applications with acceptable accuracy.

K e y w o r d s: deformation curve, hot deformation, microstructure, manganese, true strain, true stress

1. Introduction

The present paper deals with the use of dilatometry to determine the deformation resistance of lean medium-manganese steels and points to its dependence on the deformation rate and the deformation temperature. In 2003, Speer et al. [1] first proposed an approach designated as the Q&P process to exploit novel martensitic steels containing retained austenite (Q&P steel), based on the fact that carbon can diffuse from supersaturated martensite into neighbouring untransformed austenite and stabilise it to room temperature. Early investigations also proposed a corresponding thermodynamic model for Q&P steel and its heat treatment, which is now referred to as constrained carbon equilibrium [2]. Many researchers [3–10] have investigated the relationship between properties and microstructures of Q&P steels subjected to various heat treatments and showed that the ultra-high strength of Q&P steel results from martensite laths, while its good ductility is attributed to TRIP-assisted behaviour of retained austenite during deformation. De Moor et al. [11] examined the stability of retained austenite and showed that the TRIP effect occurs in Q&P steels, thereby effectively contributing to the significant strain hardening. Santofimia et al. [12] and Takahama et al. [13] analysed microstructural evolution during annealing by using a model considering the influence of martensite–austenite interface migration on the kinetics of carbon partitioning and indicated that different interface mobilities lead to profound differences in the evolution of microstructures during the partitioning process. In addition, processing opportunities for Q&P steels were discussed by Matlock and Speer [14] and Thomas et al. [15, 16] based on the considerations in the appli-

*Corresponding author: e-mail address: igor.barenyi@tnuni.sk

Table 1. Chemical composition of the 0.2C3Mn1.5Si examined steel (wt.%)

Element	C	Mn	Si	P	S	Al
Min	0.195	2.95	1.45	–	–	–
Max	0.205	3.05	1.55	0.01	0.005	0.05
Spectral analysis	0.196	2.96	1.46	0.007	0.001	0.04

cation of the Q&P concept to automotive AHSS production.

Standard medium-manganese alloyed steels with Mn content between 3 to 12 wt.% belong to the 3rd generation of advanced high strength steels used in the automotive industry. The microstructure of the steels consists of metastable retained austenite (about 30 vol.%) in the ferritic matrix. Metastable retained austenite transforms to martensite during forming processes of the components for the automotive industry, such as deep drawing. This mechanism, well known as the TRIP (Transformation Induced Plasticity) effect, results in an excellent combination of mechanical properties where the conjunction of tensile strength Rm and elongation A_{80} commonly exceeds 30 000 MPa%. These steels are designed to produce high strength automotive components with very complex shapes produced by deep-drawing, as are pillars and reinforcements with a purpose to protect passengers during possible car collisions.

Lean medium-Mn steels are a subgroup of medium--Mn steels with a reduced Mn content from 3 to 4.5 wt.% and carbon content limited to about 0.2 wt.%. Standard medium manganese steels are treated by intercritical annealing to achieve 70 vol.% of ferrite and 30 vol.% of retained austenite in the final microstructure. However, heat treatment of lean medium Mn steel is based on a different process named Q&P, consisting of quenching and following partitioning of carbon from martensite to retained austenite.

These steels are still in the laboratory development phase. Q&P process consists of the following basic steps: The steel is subjected to cold working and then heated to a temperature in a stable austenite area (above Ac3 line). After some holding period on that temperature (annealing temperature – T_{an}), very fast quenching occurs to the temperature below Ms, resulting in microstructures consisting of a high fraction of martensite and retained austenite (T_Q – T_{quech}). The next step is reheating the steel up to the partitioning temperature (above Ms) and holding a certain period on this temperature. By this partitioning temperature (T-partitioning), the carbon can be redistributed from martensite to austenite. As a result of TP, the martensite is tempered, and austenite becomes enriched in carbon. Therefore, the final structure consists of about 10–15 vol.% of metastable retained austenite, which allows the TRIP effect to be triggered by deformation-induced transformation of the austenite to martensite. Then, the final mechanical properties of such treated steel are as follows: tensile strength above 1100 MPa and higher elongations than conventional quenched and tempered steels (Q&T).

These steels will be used due to their high strength and good elongations in the near future, mainly as the side and anti-intrusion car body reinforcement structures (A, B, and C pillars, fenders, etc.) [17].

The primary purpose of the present paper is to investigate the impact of the hot working parameters such as temperature and deformation rate on the flow curves and material parameters of 0.2C3Mn1.5Si steel. In addition, the influence of these parameters on the microstructural evolution during hot deformation is thoroughly investigated.

2. Material and methods

The base material used in the present experiments is a lean medium-manganese Q&P steel 0.2C3Mn1.5Si foreseen to be used primarily in the automobile industry. The chemical composition of experimental samples was verified by a spectral analyser Q4 TASMAN, and it is presented in Table 1. The microstructure and mechanical properties of the cold-rolled steel subjected to the final Q&P heat treatment are thoroughly described in [18].

The base material was cast into 80 kg of ingot under laboratory conditions in a medium frequency furnace; the ingot dimensions were $80 \times 120 \times 1000\,mm^3$, followed by hot rolling to a final thickness of 6 mm. Dilatometer DIL805A/D is a laboratory device used to measure and record dilatation curves or to measure hot deformation resistance. Therefore, it is well designed for the physical modelling of hot forming processes [19–22]. An experimental sample of the prescribed shape and dimensions of ø 5 × 10 mm^2 from the as hot rolled condition is inserted into the working chamber between two ceramic jaws. An actual measurement consisted of heating the samples using the induction coil to the desired temperature at the heating rate $1\,℃\,s^{-1}$, followed by holding at the desired deformation temperature in the range of 900–1200 ℃ for 30 min. Upon completion of the soaking stage, the sample was subsequently compressed by a hydraulic cylinder using the desired deformation rate in the range of $0.01–10\,s^{-1}$. The en-

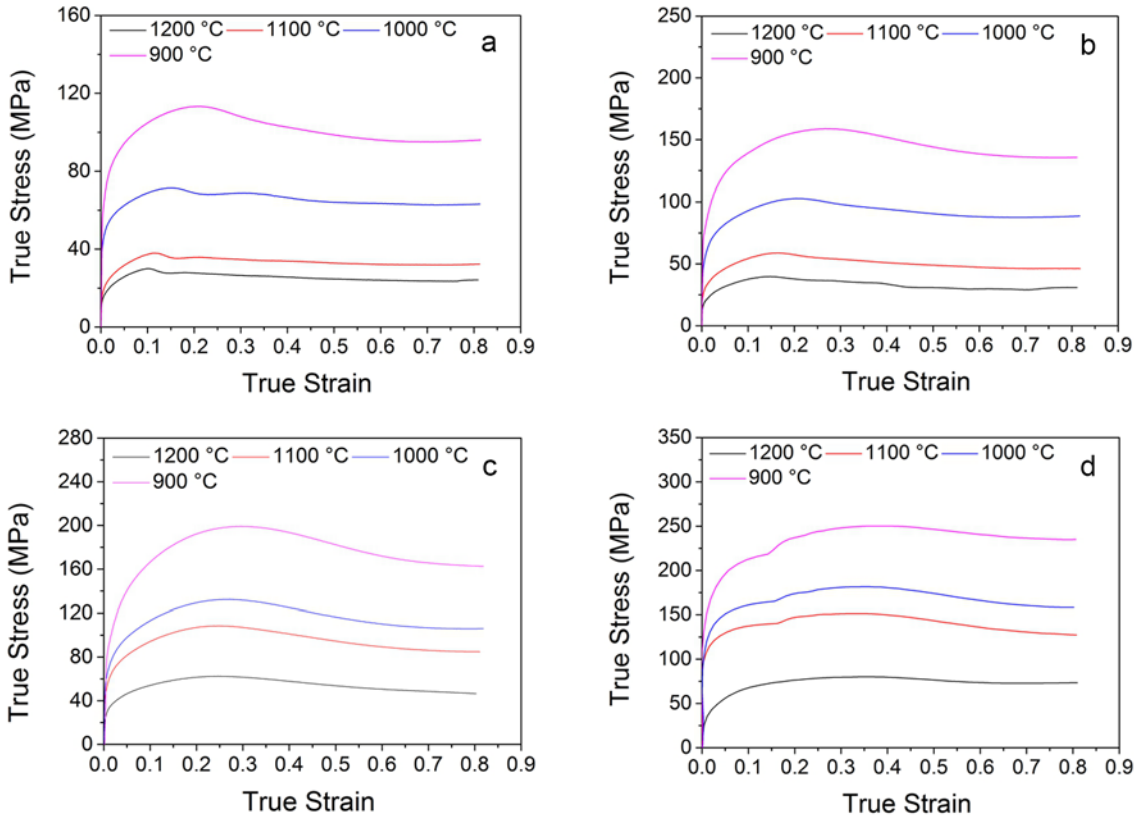

Fig. 1. True stress-strain curves of high-strength steel 0.2C3Mn1.5Si under different strain rates: (a) $\dot{\varepsilon} = 0.01\,s^{-1}$, (b) $\dot{\varepsilon} = 0.1\,s^{-1}$, (c) $\dot{\varepsilon} = 1\,s^{-1}$, and (d) $\dot{\varepsilon} = 10\,s^{-1}$.

tire heating and deformation process took place in a vacuum of 5–10 millibar. After the deformation stage, each sample was cooled at 50 °C s^{-1} by an inert gas (He). The cooling rate of all samples after deformation was set to 20 °C s^{-1}. Based on the force required to overcome the deformation resistance of the sample, we created the resulting true stress-true strain high-temperature flow curves for each tested combination of temperature and strain rate. The microstructure of each sample was evaluated using LOM. The samples were etched by a 3% Nital etchant.

A different approach was used to prepare the samples for grain size measurement. The quenched specimens after deformation were sliced along the axial section. The sections were polished and etched in a solution of picric acid (5 g) + H_2O (100 ml) + HCl (2 ml) + benzene sulfonic acid (2 g) at 50 °C for 3–4 min. Then, the optical micrographs were recorded in the centre region of the samples using a metalloscope, and the average recrystallised grain size of specimens was measured using the software Image-Pro Plus, according to the line interception method described in ASTM E112-96 standards.

3. Results

3.1. True stress-strain behaviour and microstructure of 0.2C3Mn1.5Si steel

The flow curves of lean medium-manganese of 0.2C3Mn1.5Si steel at different temperatures and strain rates are displayed in Fig. 1. All curves show a rapid increase in the flow stress due to a pronounced work hardening in the first phase of compression [23, 24]. It is also noticeable that the flow stress decreases with an increase in temperature or a decrease in deformation rate due to a dynamic recovery (DRV). This effect was also observed in [25]. All curves have single peak stress in the range of 0 to 0.9 deformations, resulting from dynamic recrystallisation (DRX). The peak stresses were obtained for all flow curves in a deformation range of 0.1–0.3. When peak stress is reached, true stress decreases with increasing deformation due to softening mechanisms [26]. In the case of higher temperatures (1100–1200 °C), it can be stated that there has been reached a balance between softening and hardening mechanisms, and the steady-state stress has been achieved from deformations above 0.5. Moreover, in a temperature range of 900–1000 °C in the deformation's region of about 0.6–0.7, the harden-

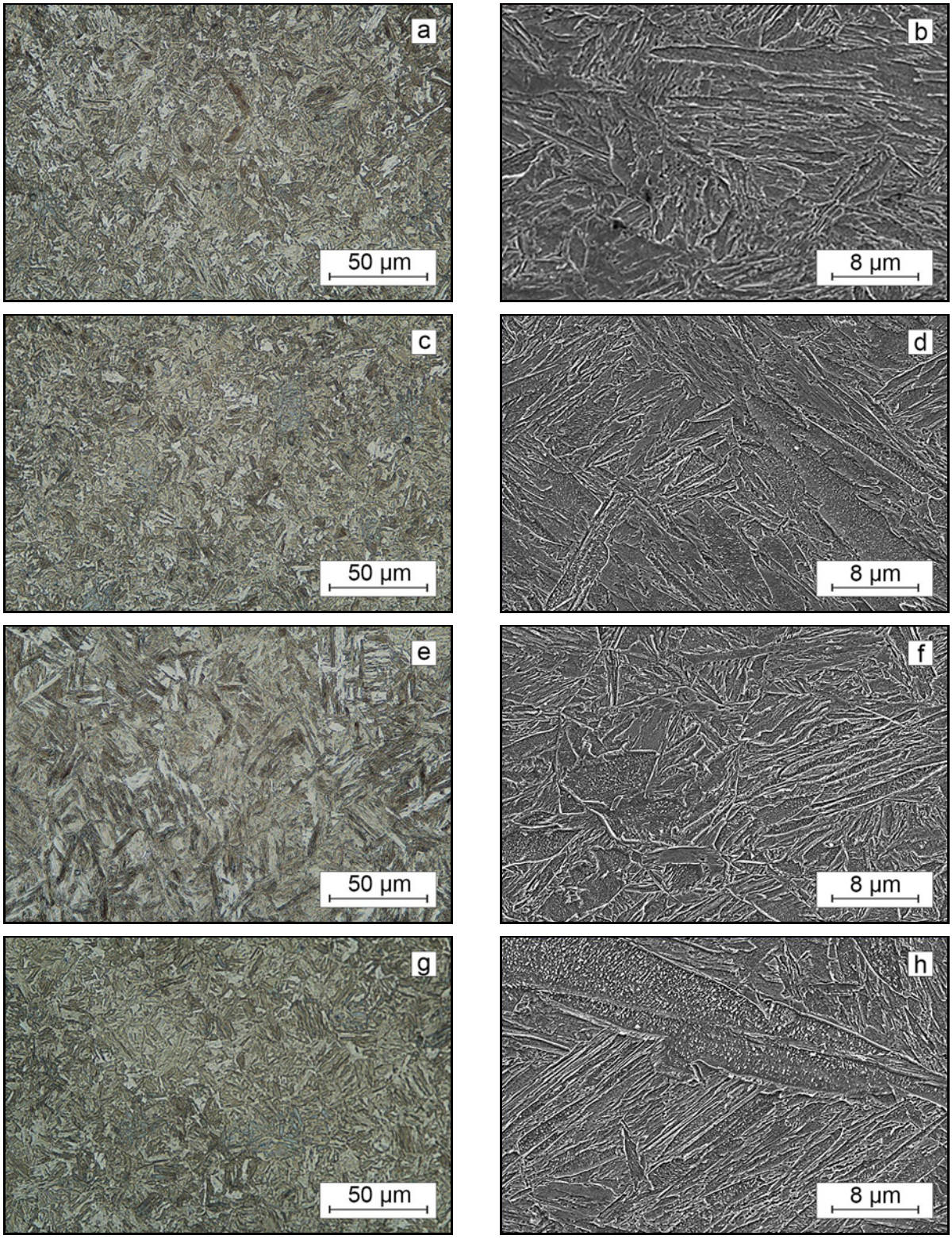

Fig. 2a–h. Microstructure of specimens obtained by LOM and SEM: temperature of 900 °C, strain rate of 0.01 s^{-1} – (a) LOM, (b) SEM; temperature of 900 °C, strain rate of 10 s^{-1} – (c) LOM, (d) SEM; temperature of 1000 °C, strain rate of 0.01 s^{-1} (near the outer surface) – (e) LOM, (f) SEM; temperature of 1000 °C, strain rate of 10 s^{-1} – (g) LOM, (h) SEM.

ing mechanism again begins to prevail, resulting in a slight rise of the flow curves.

The microstructure of the selected samples refers to the limiting temperature conditions and the deformation rates in Fig. 2. All microstructures contain tempered martensite formed upon final cooling. Obvi-

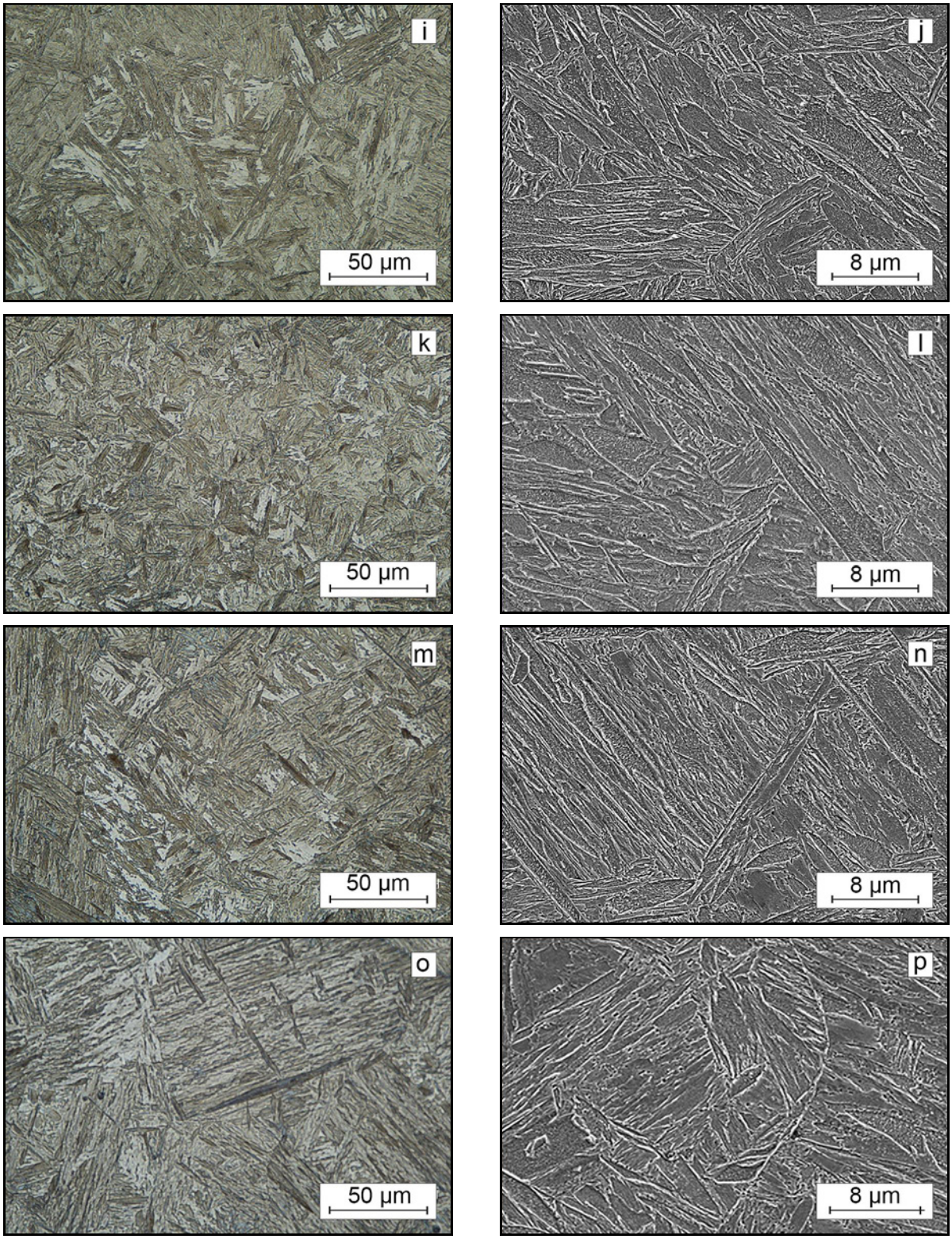

Fig. 2i–p. Microstructure of specimens obtained by LOM and SEM: temperature of 1100 °C, strain rate of 0.01 s^{-1} – (i) LOM, (j) SEM; temperature of 1100 °C, strain rate of 10 s^{-1} – (k) LOM, (l) SEM; temperature of 1200 °C, strain rate of 0.01 s^{-1} – (m) LOM, (n) SEM; temperature of 1200 °C, strain rate of 10 s^{-1} – (o) LOM, (p) SEM.

ously, with increasing deformation rate and decreasing deformation temperature, the microstructure tends to refine and vice versa. The refinement at lower temperatures and higher deformation rates is a consequence of the DRX process confirmed by quantitative analysis of grain size. This holds for both primary austenite

grains size as well as the bath size of tempered martensite.

3.2. Constitutive modelling

The Arrhenius equation, a phenomenological approach, was used to predict the constitutive equation [27, 28], which gives the flow stress and strain at different temperatures and expresses the Z parameter, known as the Zener-Hollomon parameter [29]. The Z parameter represents the temperature compensated strain rate, which has been widely used to characterise the behaviour of materials in hot working [30]. The Z parameter is formulated as:

$$Z = \dot{\varepsilon} \exp\left(-\frac{Q}{R_G T}\right), \tag{1}$$

where $\dot{\varepsilon}$ is the strain rate, T is the temperature in K, R_G is the gas constant ($R = 8.314\,\mathrm{J\,mol^{-1}\,K^{-1}}$), and Q is the activation energy. The strain rate can be expressed:

$$\dot{\varepsilon} = AF(\sigma) \exp\left(-\frac{G}{R_G T}\right), \tag{2}$$

where

$$F(\sigma) = \begin{cases} \sigma^{n'} & (\alpha\sigma < 0.8), \\ \exp(\beta\sigma) & \text{For all } \sigma, \\ [\sinh(\alpha\sigma)]^n & (\alpha\sigma > 1.2), \end{cases} \tag{3}$$

where A, n', β, α, and n are the material constants. These constants can be directly determined from experimental data obtained by the hot compression test. The following section will give the calculation procedure to obtain the material constants for the peak stress. For the low flow stress level ($\alpha\sigma < 0.8$) and the high-stress level ($\alpha\sigma > 1.2$), the relationship between the flow stress and strain rate can be expressed as the power-law and exponential law of $F(\sigma)$ in Eq. (2), respectively. Thus, the correlation between low and high stress can be as follows:

$$\dot{\varepsilon} = B\sigma^{n'} \quad (\text{for } \alpha\sigma < 0.8), \tag{4}$$

$$\dot{\varepsilon} = B' \exp(\beta\sigma) \quad (\text{for } \alpha\sigma > 1.2), \tag{5}$$

where B and B' are material constants independent of the deformation temperature. After logarithmization in the Eqs. (4) and (5) one obtains:

$$\ln(\sigma) = \frac{1}{n'} \ln(\dot{\varepsilon}) - \frac{1}{n'} \ln(B), \tag{6}$$

$$\sigma = \frac{1}{\beta} \ln(\dot{\varepsilon}) - \frac{1}{\beta} \ln(B'). \tag{7}$$

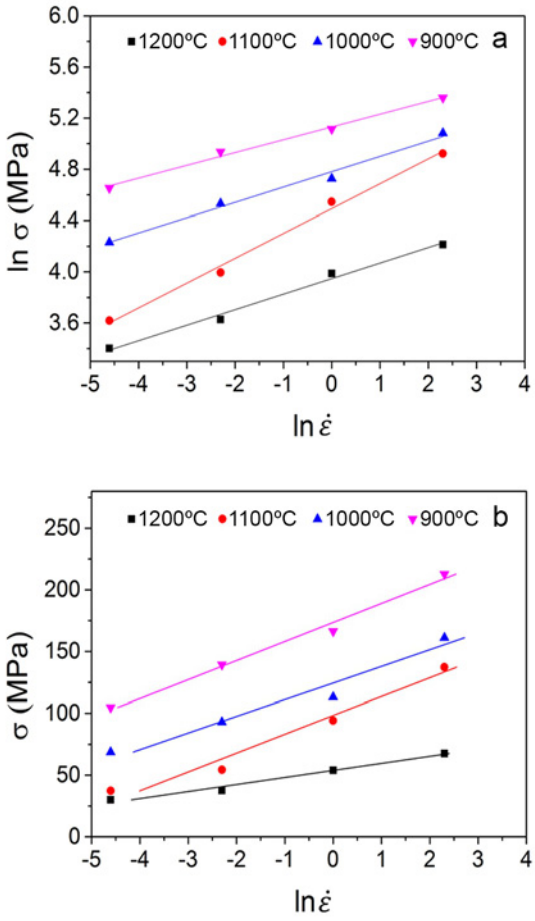

Fig. 3. (a) Relationship between $\ln(\sigma)$ and $\ln(\dot{\varepsilon})$ for derivation of n' parameter, (b) relationship between σ *vs* $\ln(\dot{\varepsilon})$ for the derivation of the β parameter.

Based on Eqs. (6) and (7), it is possible to determine the parameters n' and β from the graphical dependences $\ln(\sigma)$ vs $\ln(\dot{\varepsilon})$ and σ vs $\ln(\dot{\varepsilon})$, substituting for the stress values the peak stress values of the respective strain rates and temperatures. Then, the parameters will be defined as:

$$n' = \left[\frac{\partial \ln \dot{\varepsilon}}{\partial \ln \sigma}\right]_T, \tag{8}$$

$$\beta = \left[\frac{\partial \ln \dot{\varepsilon}}{\partial \sigma}\right]_T. \tag{9}$$

The value of the parameter n' is obtained as the reciprocal value of the slope in the $\ln(\sigma)$ vs $\ln(\dot{\varepsilon})$ plot (Fig. 3a) and the parameter β as the reciprocal value of the slope in the σ vs $\ln(\dot{\varepsilon})$ plot (Fig. 3b). It is obvious from the graphical dependences that the respective points can be linearly fitted, whereby fitting the lines for individual temperatures have a similar slope.

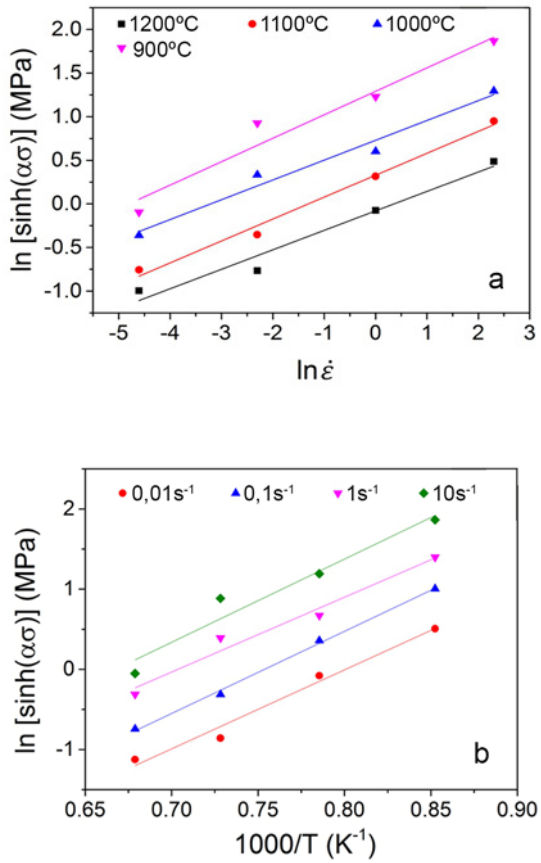

Fig. 4. (a) Relationship between $\ln[\sinh(\alpha\sigma)]$ *vs* $\ln(\dot{\varepsilon})$ for obtaining n parameter, (b) relationship between $\ln[\sinh(\alpha\sigma)]$ *vs* $1000/T$ for obtaining Q parameter.

Subsequently, the mean peak stress values will be determined as the average values of the slopes, which are supposed to be temperature independent, namely $n' = 7.534 \pm 0.5589$ and $\beta = 0.07878 \pm 0.00651$. Consequently, the α parameter is $\alpha = \beta/n' = 0.0105$.

For all stress levels (low and high), Eq. (2) can be represented as follows:

$$\dot{\varepsilon} = A\left[\sinh(\alpha\sigma)\right]^n \exp\left(-\frac{Q}{R_\mathrm{G}T}\right). \tag{10}$$

By logarithmization the Eq. (10), the following equation can be obtained:

$$\ln\left[\sinh(\alpha\sigma)\right] = \frac{\ln\dot{\varepsilon}}{n} + \frac{G}{nR_\mathrm{G}T} - \frac{\ln A}{n}. \tag{11}$$

By differentiating the Eq. (11) at a constant temperature, it can be written:

$$\frac{1}{n} = \left[\frac{\partial \ln\left[\sinh(\alpha\sigma)\right]}{\partial \ln(\dot{\varepsilon})}\right], \tag{12}$$

where the value of n is again determined as the reciprocal value of the average values of the slopes of the linear fitting in the graphical dependence $\ln[\sinh(\alpha\sigma)]$ vs $\ln(\dot{\varepsilon})$ for each temperature (Fig. 4a), and its value is $n = 3.9$ with a standard error of 0.018. According to Eq. (10), for given deformation rates, it is possible to construct the graphical dependences $\ln[\sinh(\alpha\sigma)]$ vs $1000/T$ (Fig. 4b). The slopes of the individual linear fittings form $Q/R_\mathrm{G}n$ values, and thus the hot deformation activation energy values Q can be determined. Its average value is $300.88\,\mathrm{kJ\,mol^{-1}}$. For comparison, in the study of Choudhary [31], the energy for austenitic stainless steel was determined to be $Q = 206\,\mathrm{kJ\,mol^{-1}}$, and for the magnesium alloy in the study of Dong [32], the value was $Q = 156.14\,\mathrm{kJ\,mol^{-1}}$. Krbata et al. [33] derived $Q = 305.84\,\mathrm{kJ\,mol^{-1}}$ for X153CrMoV12 high strength steel activation energies that were associated with the peak stress.

From this graphical dependence $\ln[\sinh(\alpha\sigma)]$ vs $\ln(\dot{\varepsilon})$, the parameter $\ln A$ can also be derived from the intercept of the linear fitting according to:

$$\ln A = \frac{Q}{R_\mathrm{G}T} + \frac{C'}{n}, \tag{13}$$

where parameter C' represents the intercepts of the linear fitting for each temperature. Using this approach, the $\ln A$ parameter for the respective temperature is obtained, and their mean value is $\ln A = 24.85$. Subsequently, using Eq. (1), the peak flow stress value can be expressed taking into consideration Eq. (10):

$$\sigma_\mathrm{p} = \frac{1}{\alpha}\left\{\left(\frac{\dot{\varepsilon}\exp\left(\frac{Q}{R_\mathrm{G}T}\right)}{A}\right)^{\frac{1}{n}} + \left[\left(\frac{\dot{\varepsilon}\exp\left(\frac{f_3(\varepsilon)}{R_\mathrm{G}T}\right)}{A}\right)^{\frac{2}{n}} + 1\right]^{\frac{1}{2}}\right\}. \tag{14}$$

Similar to the material parameters for peak stresses, these parameters can also be determined for the entire strain range. In this case, all of the parameters were calculated for the strain from 0.1 to 0.8 with the step of 0.05. To predict the flow stress over a wide range of temperatures and strains, it is necessary to interpolate the obtained values by a specific continuous function. Strain-dependent material parameters are often translated by a polynomial curve of a certain degree [34–36]. To select the polynomial degree correctly, we fitted obtained points by the polynomials from the 2nd to 7th order, and based on the quality of fitting, represented by the coefficient of determination R^2, the final decision for an appropriate equation selection could be made. The polynomial of 3rd order is sufficient to correctly determine the α, n, Q, and A parameters since at higher polynomial, the fitting accuracy increased negligibly. Finally, the material parameters can be expressed using the following

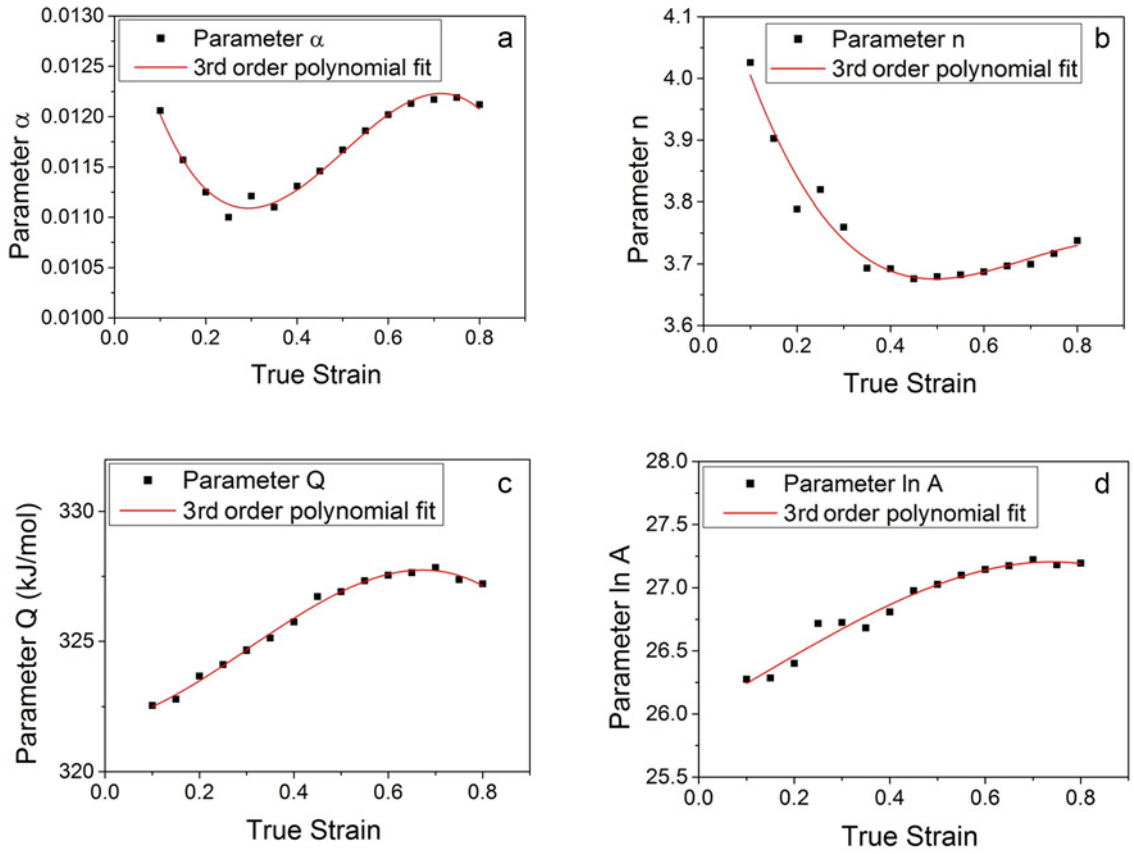

Fig. 5. Material parameter dependence in full range of strain, (a) parameter α, (b) parameter n, (c) parameter Q, and (d) parameter ln A.

equations (15)–(18):

$$\alpha = D_0 + D_1\varepsilon + D_2\varepsilon^2 + D_3\varepsilon^3, \quad (15)$$

$$n = E_0 + E_1\varepsilon + E_2\varepsilon^2 + E_3\varepsilon^3, \quad (16)$$

$$Q = F_0 + F_1\varepsilon + F_2\varepsilon^2 + F_3\varepsilon^3, \quad (17)$$

$$\ln A = G_0 + G_1\varepsilon + G_2\varepsilon^2 + G_3\varepsilon^3. \quad (18)$$

In Fig. 5, it can be seen the evolution of individual material parameters depending on the true strain in the range from 0.1 to 0.8. It is evident from the polynomial fitting that the strain has a significant influence on the evolution of the parameters and when predicting the true stress during hot deformation, it is necessary to use the functional dependence of these parameters, not just a specific value. After determining the material parameters using functional equations, it is possible to express the Arrhenius equation (Eq. (14)) for different strain and temperature values as follows:

$$\sigma = \frac{1}{f_1(\varepsilon)}\left(\frac{\dot{\varepsilon}\exp\left(\frac{f_3(\varepsilon)}{R_G T}\right)}{\exp\left[f_4(\varepsilon)\right]}\right)^{\frac{1}{f_2(\varepsilon)}} + \frac{1}{f_1(\varepsilon)}\left[\left(\frac{\dot{\varepsilon}\exp\left(\frac{f_3(\varepsilon)}{R_G T}\right)}{\exp\left[f_4(\varepsilon)\right]}\right)^{\frac{2}{f_2(\varepsilon)}} + 1\right]^{\frac{1}{2}}, \quad (19)$$

where the values of $f_i(\varepsilon)$ (i = 1, 2, 3, 4) represent the individual polynomial functions of the material parameters depending on the applied strain.

3.3. Grain size measurement

Light microscopy has been selected to observe microstructure evolution for all used deformation parameters. Figures 6a,b show the microstructure of 0.2C3Mn1.5Si steel deformed at a constant strain rate of 1 s^{-1} and the temperature of 900 and 1200 ℃. For the increased deformation temperature of 1200 ℃, the growth of the grains turned to be easier. As shown in Fig. 6b, big grains were formed, and tiny grains between the grain boundaries were observed, which indicated the growth of recrystallised grains. It was pointed that because recrystallisation activation energy increased with deformation temperature, dislocation motion and crystal slip were promoted, which enhanced grain-boundary migration, facilitating nu-

Table 2. Average dynamic recrystallisation grain size (μm)

Temperature (°C)	0.01 s^{-1}	0.1 s^{-1}	1 s^{-1}	10 s^{-1}
900	13.43	8.51	5.73	3.96
1000	25.76	19.73	11.88	8.64
1100	48.76	36.58	22.92	16.28
1200	84.24	62.69	39.11	32.66

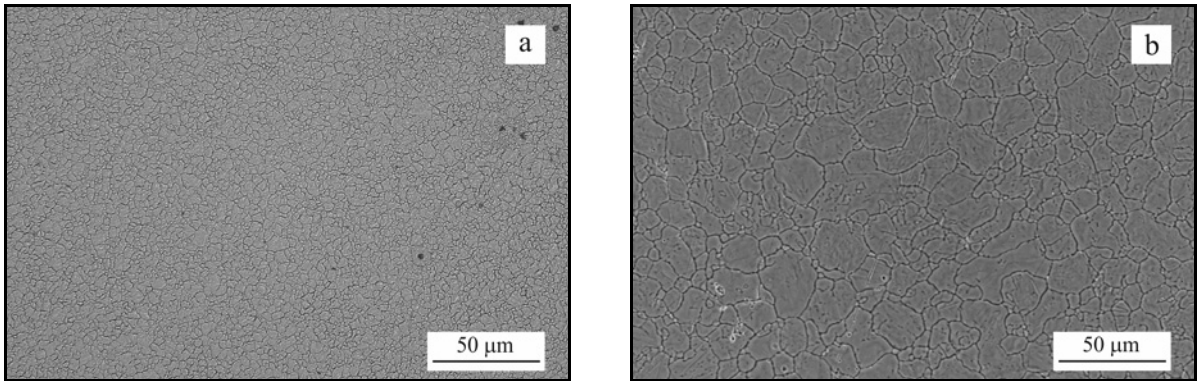

Fig. 6. Microstructure of 5CrNiMoV steel with strain rate 1 s^{-1} etched for grain size observation: (a) $T = 900$ °C and (b) $T = 1200$ °C.

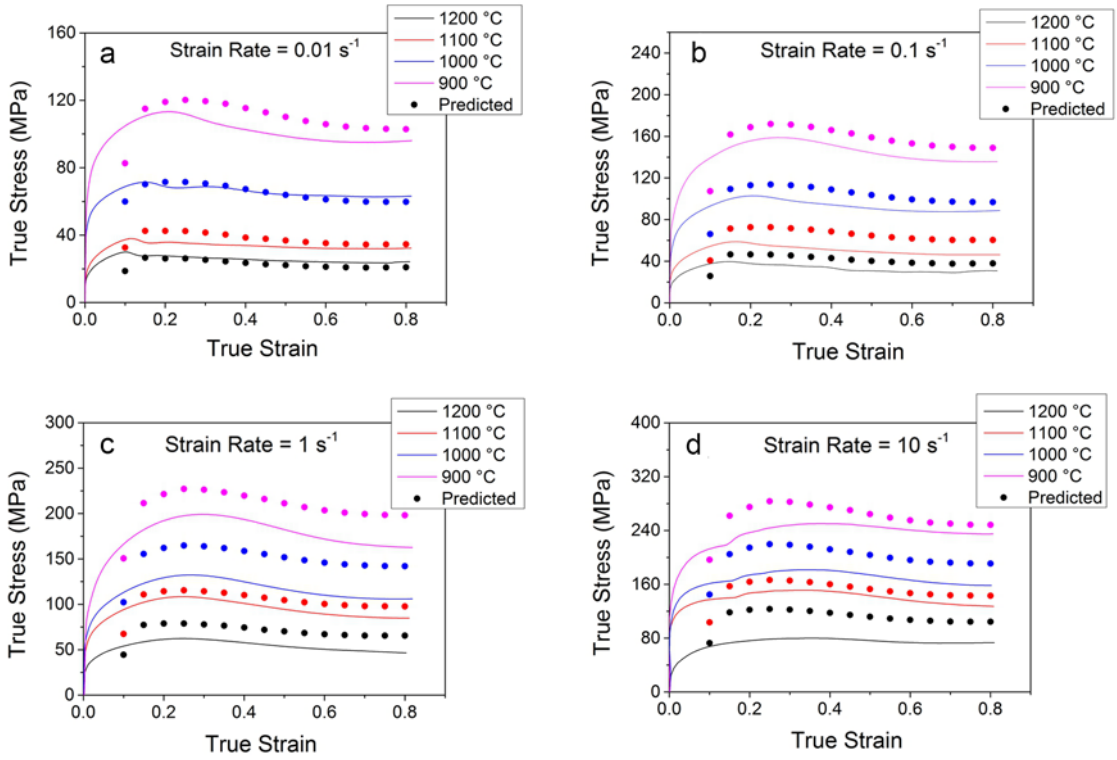

Fig. 7. Comparison between measured and predicted flow stresses of 0.2C3Mn1.5Si steel, (a) $\dot{\varepsilon} = 0.01\ s^{-1}$, (b) $\dot{\varepsilon} = 0.1\ s^{-1}$, (c) $\dot{\varepsilon} = 1\ s^{-1}$, and (d) $\dot{\varepsilon} = 10\ s^{-1}$.

cleation and growth of DRX grains [37]. In summary, although it was possible to cause incomplete recrystallisation by reducing the temperature of hot deformation or increasing the strain rate, it showed a favourable impact on grain refinement when complete recrystallisation occurred.

It was observed that the total DRX grain size usually increased with the increase of the deforma-

tion temperature or the decrease of the strain rate. The average dynamic recrystallisation grain size of 5CrNiMoV steel at different deformation conditions was measured by the quantitative metallography method according to the ASTM E112-96 standard. The measured results are listed in Table 2. The average grain size of dynamic recrystallisation depends on the deformation temperature and the strain rate.

4. Discussion

A comparison of the measured data with the data obtained by the constitutive model is shown in Fig. 7. The present comparison was carried out for the deformation rates from 0.01 to 10 s^{-1} and deformation temperatures from 900 to 1200 ℃. It is clear that at a strain rate of 0.01 s^{-1}, the difference between the measured and predicted data is minimal. In other conditions, the experimental and predicted data are in relatively good agreement.

For an overall assessment of the applicability of the given constitutive model for 0.2C3Mn1.5Si steel, the coefficient of determination R^2 and MAPE (Mean Absolute Average Error) were calculated for the flow stress values at all deformation rates and temperatures. Statistic parameter MAPE is calculated by the equation:

$$\mathrm{MAPE} = \frac{1}{N}\sum_{i=1}^{N}\left|\frac{\sigma_\mathrm{E}-\sigma_\mathrm{M}}{\sigma_\mathrm{E}}\right| \times 100, \qquad (20)$$

where N is the data number, σ_E and σ_M are experimental and predicted flow stress, respectively. The correlation dependence between measured and predicted flow stress is shown in Fig. 8. The values of the R^2 and MAPE are 0.905 and 19.06 %, respectively. The value of the coefficient of determination shows that the prediction of stress values by the constitutive model is at an acceptable level. The value of the MAPE parameter also, according to [38], speaks of a good to sufficient quality of prediction by the presented model.

As shown, the above procedure for obtaining material constants into the constitutive model based on the Zener-Hollomon parameter can also be used in the case of high-strength steel 0.2C3Mn1.5Si. This model can predict flow stress in a relatively large range of deformation rates and temperatures. The boundaries where the model already shows large differences with experimental data are very low deformation rates ($\approx 0.01\ s^{-1}$) or large deformation rates ($\approx 10\ s^{-1}$) at deformation temperatures of about 900 ℃. This may be related to the fact that these parameters do not cause any structural changes in the materials. Therefore, it can be said that this model is better suited in cases where the materials undergo microstructural changes.

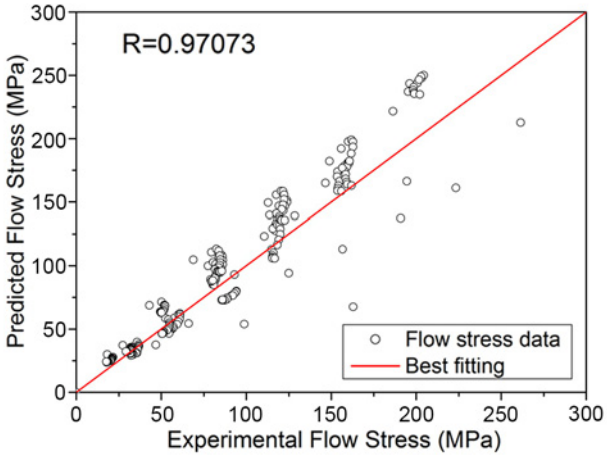

Fig. 8. The correlation between predicted and measured flow stresses for all measurements.

The flow curves of the investigated material generally exhibit signs of DRX with a broad peak that is different to the plateau, characteristic of a material that undergoes only dynamic recovery. This was also confirmed by the microstructural examination of this material, where coarse martensitic laths were formed in a temperature range from 1000–1200 ℃ after cooling, as opposed to significant grain refinement at a lower temperature of 900 ℃.

Variations and inaccuracies were caused by the inaccuracy of the model itself, the linear fitting of the material constants. The change in material structure also significantly impacts the stress-strain relationship as a function of the grain size [39]. In other areas of deformation and temperature, the model is relatively well correlated with experimental data, thus determining the interval at which the model is applicable. Another indicator of the suitability of the model for this material is that the material parameters could be approximated by the polynomial function of the 3rd or the 5th order, respectively, while in other works, polynomial functions of the 6th or the 7th order must be applied.

5. Conclusions

In this work, deformation analysis of high strength lean-manganese Q&P steel 0.2C3Mn1.5Si at high temperature was investigated at deformation temperatures from 900 to 1200 ℃ and strain rates from 0.01 to 10 s^{-1}. Constructed flow curves were evaluated using a constitutive model based on the Zener-Hollomon parameters.

The following conclusions can be drawn from the present work:

1. 0.2C3Mn1.5Si steel exhibits DRX with single peak stress in the entire range of temperatures and deformation rates. A typical flow stress curve with DRX is more recognisable at higher temperatures and lower strain rates, and the flow stress level increases with increasing strain rate and decreasing deformation temperature. When peak stress is reached, softening mechanisms start to prevail, which, at higher deformation temperatures, is balanced with the hardening mechanisms. Finally, the steady-state stress stabilises the flow stress. In the case of lower temperatures, where the peak stress is also significant, there is also a significant DRX process in play. Therefore, a significantly refined structure could be observed using the LOM technique.

2. With the constitutive model and flow curves, it is possible to obtain material parameters and thus predict true stress and strain behaviour in a wide range of temperatures and deformation rates. Material parameters can be obtained by polynomial fitting of the 3^{rd} and 5^{th} order, respectively, preserving a particular physical meaning of the parameters while maintaining relative mathematical simplicity.

3. The derived hot deformation activation energy $Q = 300.88\,kJ\,mol^{-1}$ falls well into the range of the hot deformation activation energies known from other high strength steel. Also, the measured activation energy value is close to the self-diffusion activation energy of iron ($285\,kJ\,mol^{-1}$), which supports the dominancy of the DRX mechanism in terms of activation energy as well.

4. The flow stress prediction using the above procedure is in acceptable agreement with the experimental flow stress patterns as the correlation in Fig. 8 between experimental versus predicted flow stress individual values has shown. Such a result, along with a graphical comparison of predicted and measured flow stress curves, allows the use of a constitutive model to predict the flow curves during hot deformation (e.g., hot rolling) for these types of high strength steel.

5. Quantitative microscopy results indicated that DRX was the primary mechanism of work softening for steels during large deformation, and austenite grains were significantly refined by reducing the temperature of hot deformation or increasing the strain rate when complete recrystallisation occurred.

Acknowledgements

This work was supported by the Slovak Research and Development Agency under contract no. APVV-15-0710 and by the Science Grant Agency under project no. 1/0346/19.

This publication was created in the frame of the project: Advancement and support of R&D for "Centre for diagnostics and quality testing of materials" in the domains of the RIS3 SK specialization, ITMS2014+: 313011W442, based on the Operational Programme Integrated Infrastructure and funded from the European Regional Development Fund.

References

[1] J. G. Speer, D. K. Matlock, B. C. DeCooman, J. G. Schroth, Carbon partitioning into austenite after martensite transformation, Acta Mater. 51 (2003) 2611–2622. doi:10.1016/S1359-6454(03)00059-4

[2] J. G. Speer, D. K. Matlock, B. C. DeCooman, J. G. Schroth, Comments on "On the definitions of paraequilibrium and orthoequilibrium" by M. Hillert and J. Agren, Scr. Mater. 50 (2004) 697–699. doi:10.1016/j.scriptamat.2004.08.029

[3] J. G. Speer, F. C. Rizzo Assunção, D. K. Matlock, D. V. Edmonds, The quenching and partitioning process: background and recent progress, Mater. Res. 8 (2005) 417–423. doi:10.1590/S1516-14392005000400010

[4] D. V. Edmonds, K. He, M. K. Miller, F. C. Rizzo, A. Clarke, D. K. Matlock, J. G. Speer, Microstructural features of quenching and partitioning: A new martensitic steel heat treatment, Proceedings of 5th International Conference on Processing and Manufacturing of Advanced Materials (2006), pp. 4819–4825. ISBN 9781605601052

[5] D. V. Edmonds, K. He, F. C. Rizzo, B. C. De Cooman, D. K. Matlock, J. G. Speer, Quenching and partitioning martensite – A novel steel heat treatment, Mater. Sci. Eng. A 438–440 (2006) 25–34. doi:10.1016/j.msea.2006.02.133

[6] K. He, D. V. Edmonds, J. G. Speer, D. K. Matlock, F. C. Rizzo, Microstructural characterisation of steel heat-treated by the novel quenching and partitioning process, Proceedings of 14th European Microscopy Congress, EMC 2008, (2008), pp. 429–430. ISBN: 978-3-540-85228-5

[7] S. S. Nayak, R. Anumolu, R. D. K. Misra, K. H. Kim, D. L. Lee, Microstructure-hardness relationship in quenched and partitioned medium-carbon and high-carbon steels containing silicon, Mater. Sci. Eng. A 498 (2008) 442–456. doi:10.1016/j.msea.2008.08.028

[8] M. J. Santofimia, L. Zhao, R. Petrov, J. Sietsma, Characterisation of the microstructure obtained by the quenching and partitioning process in a low-carbon steel, Mater. Charact. 59 (2008) 1758–1764. doi:10.1016/j.matchar.2008.04.004

[9] C. Y. Wang, J. Shi, W. Q. Cao, H. Dong, Characterisation of microstructure obtained by quenching and partitioning process in low alloy martensitic steel, Mater. Sci. Eng. A 527 (2010) 3442–3449. doi:10.1016/j.msea.2010.02.020

[10] J. G. Speer, E. De Moor, K. O. Findley, D. K. Matlock, B. C. De Cooman, D. V. Edmonds, Analysis of microstructure evolution in quenching and partitioning automotive sheet steel, Metall. Mater. Trans. A 42 (2011) 3591–3601. doi:10.1007/s11661-011-0869-7

[11] E. De Moor, S. Lacroix, A. J. Clarke, J. Penning, J. G. Speer, Effect of retained austenite stabilised via quench and partitioning on the strain hardening of martensitic steels, Metall. Mater. Trans. A 39 (2008) 2586–2589. doi:10.1007/s11661-008-9609-z

[12] M. J. Santofimia, L. Zhao, J. Sietsma, Model for the interaction between interface migration and carbon

diffusion during annealing of martensite–austenite microstructures in steels, Scr. Mater. 59 (2008) 159–162. doi:10.1016/j.scriptamat.2008.02.045
[13] Y. Takahama, M. J. Santofimia, M. G. Mecozzi, L. Zhao, J. Sietsma, Phase field simulation of the carbon redistribution during the quenching and partitioning process in a low-carbon steel, Acta Mater. 60 (2012) 2916–2926. doi:10.1016/j.actamat.2012.01.055
[14] D. K. Matlock, J. G. Speer, Processing opportunities for new advanced high-strength sheet steels, Mater. Manuf. Process. 25 (2010) 7–13. doi:10.1080/10426910903158272
[15] G. A. Thomas, J. G. Speer, D. K. Matlock, Considerations in the application of the quenching and partitioning concept to hot rolled AHSS production, Iron Steel Technol. 5 (2008) 209–217.
[16] G. A. Thomas, J. G. Speer, D. K. Matlock, Quenched and partitioned microstructures produced via Gleeble simulations of hot-strip mill cooling practices, Metall. Mater. Trans. A 42 (2011) 3652–3659. doi:10.1007/s11661-011-0648-5
[17] S. Kaar, K.Schneider, D. Krizan, C. Béal, Ch. Sommitsch, Influence of the quenching and partitioning process on the transformation kinetics and hardness in a lean medium manganese TRIP steel, Metals 9 (2019) 353. doi:10.3390/met9030353
[18] S. Kaar, D. Krizan, K. Schneider, C. Béal, Ch. Sommitsch, Effect of manganese on the structure-properties relationship of cold rolled AHSS treated by a quenching and partitioning process, Metals 9 (2019) 1122. doi:10.3390/met9101122
[19] I. Barényi, M. Krbaťa, J. Majerík, I. Mikušová, Effect of deformation parameters on microstructure evolution and properties of 33NiCrMoV15 steel, IOP Conference Series: Materials Science and Engineering 776 (2020) 012001. doi:10.1088/1757-899X/776/1/012001
[20] M. Krbaťa, J. Majerík, I. Barényi, M. I. Eckert, Experimental determination of continuous cooling transformation diagram for high strength steel OCHN3MFA, IOP Conference Series: Materials Science and Engineering 776 (2020) 012095. doi:10.1088/1757-899X/776/1/012095
[21] I. Barényi, M. Krbaťa, J. Majerík, Structure evolution of 33NiCrMoV15 steel in relation to tempering temperature, DAAAM International Symposium on Intelligent Manufacturing and Automation 30 (2019) 800–805. doi:10.2507/30th.daaam.proceedings.111
[22] I. Barényi, J. Majerík, M. Krbaťa, Structure evolution of 33NiCrMoV15 steel after its processing by various quenching conditions, Procedia Structural Integrity 23 (2019) 547–552. doi:10.1016/j.prostr.2020.01.143
[23] L. Lan, W. Zhou, R. D. K. Misra, Effect of hot deformation parameters on flow stress and microstructure in a low carbon microalloyed steel, Mat. Sci. Eng. A 756 (2019) 18–26. doi:10.1016/j.msea.2019.04.039
[24] J. S. Jha, S. P. Toppo, R. Singh, A. Tewari, S. K. Mishra, Flow stress constitutive relationship between lamellar and equiaxed microstructure during hot deformation of Ti-6Al4V, J. Mater. Process. Tech. 270 (2019) 216–227. doi:10.1016/j.jmatprotec.2019.02.030
[25] H. J. McQueen, S.Yue, N. D. Ryan, E. Fry, Hot working characteristic of steels in austenitic state, J. Mater. Process. Tech. 53 (1995) 293–310. doi:10.1016/0924-0136(95)01987-P
[26] S. Solhjoo, A. I.Vakis, Y. T. Pei, Two phenomenological models to predict the single peak flow stress curves up to the peak during hot deformation, Mech. Mater. 105 (2017) 61–66. doi:10.1016/j.mechmat.2016.12.001
[27] L. Jiang, L. Fuguo, C. Jun, Constitutive model prediction and flow behavior considering strain response in the thermal processing for the TA15 titanium alloy, Materials 11 (2018) 1985. doi:10.3390/ma11101985
[28] D. Samantaray, S. Mandal, A. K. Bhaduri, A comparative study on Johnson Cook, modified Zerilli-Armstrong and Arrhenius-type constitutive models to predict elevated temperature flow behaviour in modified 9Cr-1Mo steel, Comput. Mater. Sci. 47 (2009) 568–576. doi:10.1016/j.commatsci.2009.09.025
[29] C. Zener, J. H. Hollomon, Effect of strain rate upon plastic flow of steel, J. Appl. Phys. 15 (1944) 22–32. doi:10.1063/1.1707363
[30] X. Shang, Y. Cui, M. W. Fu, A ductile fracture model considering stress state and Zener-Hollomon parameter for hot deformation of metallic materials, Int. J. Mech. Sci. 144 (2018) 800–812. doi:10.1016/j.ijmecsci.2018.06.030
[31] B. K. Choudhary, Activation energy for serrated flow in type 316L(N) austenitic stainless steel, Mat. Sci. Eng. A 603 (2014) 160–168. doi:10.1016/j.msea.2014.02.083
[32] Y. Dong, C. Zhang, X. Lu, C. Wang, G. Zhao, Constitutive equations and flow behavior of an as-extruded AZ31 magnesium alloy under large strain condition, J. Mater. Eng. Perform. 25 (2016) 2267–2281. doi:10.1007/s11665-016-2092-6
[33] M. Krbaťa, M. Eckert, D. Križan, I. Barényi, I. Mikušová, Hot deformation process analysis and modelling of X153CrMoV12 steel, Metals 9 (2019) 1125. doi:10.3390/met9101125
[34] G. Wei, X. Peng, A. Hadadzedeh, Y. Mahmoodkhani, W. Xie, Y. Yang, M. A. Wells, Constitutive modelling of Mg-9Li-3Al-2Sr-2Y at elevated temperatures, Mech. Mater. 89 (2015) 241–253. doi:10.1016/j.mechmat.2015.05.006
[35] J. Li, B. Gao, S. Tang, B. Liu, Y. Liu, Y. Wang, J. Wang, High temperature deformation behavior of carbon-containing FeCoCrNiMn high entropy alloy, J. Alloy. Compd. 747 (2018) 571–579. doi:10.1016/j.jallcom.2018.02.332
[36] M. Eckert, M. Krbata, I. Barenyi, J. Majerik, A. Dubec, M. Bokes, Effect of selected cooling and deformation parameters on the structure and properties of AISI 4340 steel, Materials 13 (2020) 5585. doi:10.3390/ma13235585
[37] Y. Cheng, H. Du, Y. Wei, L. Hou, B. Liu, Metadynamic recrystallisation behaviour and workability characteristics of HR3C austenitic heat-resistant stainless steel with processing map, J. Mater. Process. Tech. 235 (2016) 134–142. doi:10.1016%2Fj.jmatprotec.2016.04.026
[38] J. J. M. Moreno, A. P. Pol, A. S. Abad, B. C. Blasco, Using the R-MAPE index as a resistant measure of forecast accuracy, Psicothema 24 (2013) 500–506. doi:10.7334/psicothema2013.23
[39] A. H. Ammouri, G. Kridli, G. Ayoub, R. F. Hamade, Relating grain size to the Zener-Hollomon parameter for twin-roll-cast AZ31B alloy refined by friction stir processing, J. Mater. Process. Tech. 222 (2015) 301–306. doi:10.1016/j.jmatprotec.2015.02.037